Article

JOURNAL OF COMPOSITE MATERIALS

Journal of Composite Materials
2017, Vol. 51(1) 67–80

DOI: 10.1177/0021998316636456
jcm.sagepub.com
SAGE

Mechanical properties and damage characterization of triaxial braided composites in environmental conditions

Joel P Johnston, Kuang C Liu, Masoud Yekani Fard and Aditi Chattopadhyay

Abstract

Under environmental conditions, triaxial braided composites exhibit complex behavior and damage mechanisms. This paper investigates the damage mechanisms of these complex composites under varying environmental conditions. Tensile, compressive, and shear specimens of triaxial braided composite material were tested at room, hot (100°C), and hot/wet conditions (60°C/90% relative humidity). The strain field was studied using a digital image correlation system and the effect that the specimens' edges have on the strain field was quantified. For the tension specimens, the environmental conditions caused reductions in the elastic and failure properties, whereas the compression specimens exhibited degradation exclusively in the failure properties. An increase in temperature rather than humidity was found to be a driving factor for the degradation of the mechanical properties. A non-destructive, flash thermography technique was used to characterize surface/subsurface damage in the specimens. Scanning electron microscopy was conducted to determine the microstructural modes of failure.

Keywords

Triaxial braid, composite, environmental conditions, mechanical properties, failure, edge effect

Introduction

Aircraft engine components experience hot/wet soaking after a flight and, in the case of composite materials, are regarded as a limiting condition in mechanical performance.[1–5] Determination of the material integrity, in relation to mechanical performance under extreme conditions, is a necessary step of the design process for aircraft certification by the Federal Aviation Administration (FAA). Due to the beneficial traits of woven and braided composites, such as delamination prevention, these types of materials are currently being used in aircraft structures. Extensive durability studies have been performed on unidirectional carbon/epoxy composites, but only limited studies have been reported on braided composites. Bishop[3] observed that elevated temperature conditions reduced the compressive failure strength of unidirectional carbon/epoxy composites. In addition to temperature, moisture studies have been conducted on unidirectional carbon/epoxy composites using humidity-controlled chambers and circulating water baths to determine the absorption behavior of the material.[4,6] Joshi[7] compared water bath and humidity controlled experiments, and concluded that water baths accelerated the moisture absorption in unidirectional composites. They showed that moisture absorption and elevated temperatures reduced the interlaminar shear strength by as much as 25% and the tensile strength by as much as 36%. The effect of moisture absorption has been studied for the tension and compression responses[5] as well as the shear response[2] of unidirectional carbon fiber/epoxy composites. Patel and Case[1] presented tension results for woven composites which were conditioned using hygrothermal cycling and moisture absorption. Zhang et al.[8] studied the reduction in tensile and compressive

School for Engineering of Matter, Transport, and Energy, Arizona State University, USA

Corresponding author:
Joel P Johnston, School for Engineering of Matter, Transport, and Energy, Arizona State University, Engineering Research Building (ENGRC) 551 E. Tyler Mall, Tempe, Arizona, 85287, USA.
Email: Joel.Johnston@asu.edu

properties of triaxial braided composites due to microcracking induced by thermal cycling. Schambron et al.[9] conditioned braided composite specimens in saline, moisture, and elevated temperature environments for bone plate structures and studied the impact the conditioning had on the flexural properties. Kohlman et al.[10] performed hygrothermal cycling on triaxial braided composites and presented the damaging effect that the environmental conditioning had on tensile, compressive, and impact resistive properties. However, their hygrothermal cycling did not determine which stage (storage, ascent, cruise, or descent) was more detrimental to the integrity of the composite material. Additional investigations are necessary to determine the effects that each individual environmental condition has on the triaxial braid material, which is important for physics-based models and failure prediction.

Different characterization techniques have been utilized to study the mechanical properties and damage in triaxial braided composites.[11–15] Strain measurement systems, such as Moiré interferometry and digital image correlation (DIC), have been used extensively to characterize full-field strain of composite materials.[12,16–18] Rao et al.[19] used fiber Bragg grating (FBG) sensors on braided carbon/epoxy composites to measure the strain and temperature on the material. Quek et al.[20] and Smith and Swanson[21] performed testing of triaxial braided composites, with digital speckle photography, to understand the failure modes of the material under biaxial loading. Using a combination of DIC and non-destructive scanning methods, correlations have been made between the strain field and damage assessment of composites.[18,22,23] Flash thermography (FT) has been routinely used in recent studies to measure specimen thickness, defects, and thermal diffusivity in large panels with no edge or boundary condition effects.[24–27] The main focus of these studies was to characterize mechanical properties and damage in braided composites. A missing element in the current literature, however, is the examination of strain gradients and damage due to environmental conditioning of triaxial braided material.

In this study, triaxial braided polymer matrix composite specimens were tested at room, hot (100°C), and hot/wet conditions (60°C/90% relative humidity [RH]) to investigate the effects of the environmental conditioning on the tensile, compressive, and in-plane shear properties. A humidity and temperature controlled chamber was used for the hot/wet conditioned specimens. A DIC system was utilized to obtain the full-field strain on the surface of the specimens and to examine strain at the edges of the specimens. An FT technique was used to examine structural degradation in the surface and sub-surface of each specimen. Scanning electron microscopy (SEM) was performed to study the effects that the environmental conditions had on the damage mechanisms.

Table 1. Constituent mechanical properties.

Resin/fiber	Tensile strength, MPa	Young's modulus, GPa	Density, g/cm^3
T700S fibers	4900	230.0	1.80
PR-520 resin	82	4.0	1.256

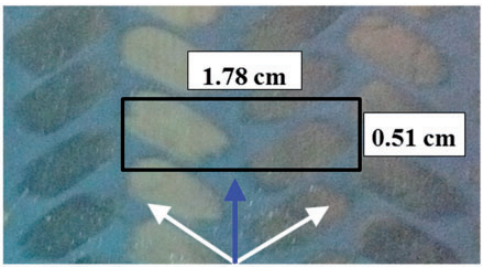

Figure 1. Architecture of the triaxial braid composite with the repeating unit cell in the outlined box (For references to color in this figure, the reader is referred to the web version of this article).

Experimental methods

Material specifications

The material in this study was a six-layer laminate of triaxial braided composite consisting of CYCOM PR-520 epoxy resin (Cytec Industries, Inc.) and TORAY T700S carbon fibers (Toray Carbon Fibers America, Inc.) with a total thickness of 3.175 mm. The constituent properties, reported by the manufacturers, are presented in Table 1. The composite material was manufactured by North Coast Composites using a resin-transfer molding technique. A 0°/ +60°/ –60° triaxial braid architecture was used and the top view of the repeating unit cell (RUC) is defined by the outlined box and dimensions in Figure 1. The blue vertical arrow in the figure indicates the direction of the axial fiber tows and the other white arrows indicate the bias braid tows oriented in the ±60° directions. The fiber volume fraction of the composite material was measured by the resin burn-off technique detailed in Procedure G of the American Society for Testing and Materials (ASTM) D3171 standard.[28] The average fiber volume fraction value determined from the experiments was 54%.

Specimen geometries

ASTM standards (D3410, D3039, D7078)[29–31] were used to guide the design of the compression, tension,

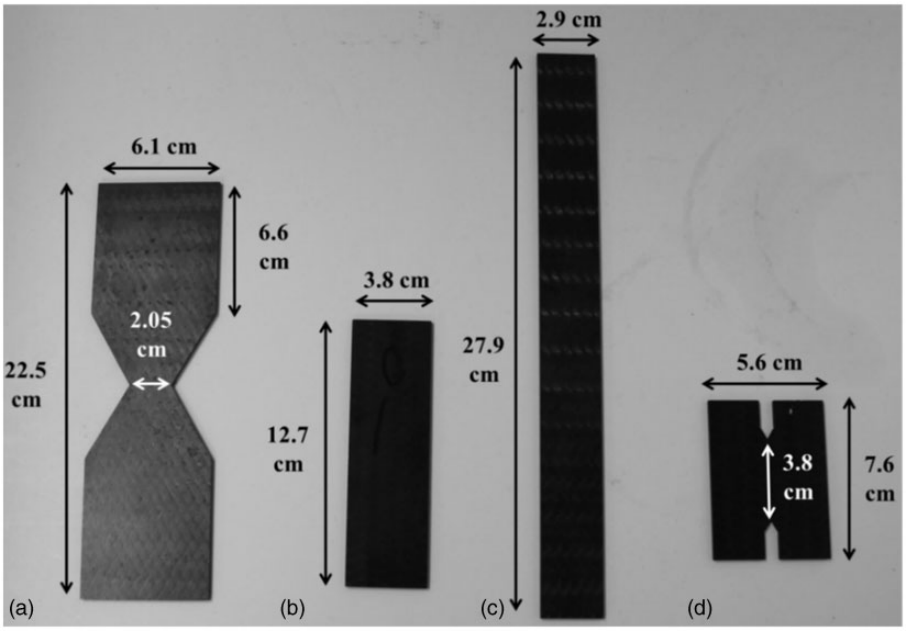

Figure 2. Average dimensions of the geometries for (a) transverse bowtie, (b) compression, (c) tension, and (d) v-notched rail shear specimens.

and shear specimens. The averaged dimensions for the specimen geometries are displayed in Figure 2. Tension and compression tests were performed for both axial (parallel to 0° axial tows) and transverse (perpendicular to 0° axial tows) directions. However, results from previous studies[11,18,32] have shown that the ASTM 3039 geometry yields premature damage and lower strength in transverse tension specimens due to the large size of the RUC and specimen edge effects. Notched[32] and bowtie[33] specimens have been tested in past studies in order to improve the transverse tensile results. Although higher strengths were noted for the notched geometry, the specimen contained a non-uniform gage region which resulted in a sharp stress concentration. In this study, a version of the bowtie geometry presented by Bowman et al.[33] was used to examine the transverse tension response and edge effects.

Experimental procedure

The specimens were tested using an Instron 5985 test frame in displacement control at a constant rate of 0.635 mm/min. A two-camera DIC system (GOM ARAMIS 2M) was time-synchronized with the test frame to study strain field through non-contact measurements. The DIC software uses pattern recognition algorithms to calculate deformation and strain at each stage by correlating the data with a reference stage.[34] A selected area of the strain field, with approximately 250 data points, was used to calculate the averaged global strain. The design of an ASTM D3410 fixture (shown in Figure 3) was modified in order to accommodate the DIC strain measurement during compression testing. Compression specimens were gripped by lateral pressure applied through the tapered slots. Bolts (shown in Figure 3b) were used for alignment and to apply initial pressure on the surface of the specimen to prevent slipping.

The following three environmental conditions were applied to the specimens: (i) room condition, (ii) hot (100°C), and (iii) hot/wet condition (60°C/90% RH). The guidelines outlined in the ASTM D5229 standard[35] were followed for the hot/wet process which consisted of conditioning the specimens in an environmental chamber for 12 weeks. Figure 4 illustrates the average weight gain which was measured to assess the moisture absorption of the material. The average weight gain due to moisture was 0.45% at the end of hot/wet conditioning. A removable thermal chamber on the mechanical frame enabled the simultaneous heating (100°C) and testing for the hot and hot/wet conditions.

A non-destructive, pulsed FT technique was performed to determine intrinsic flaws and damage on the surface and sub-surface of the specimens. The FT technique was performed using an EchoTherm system (Thermal Wave Imaging, Inc.) with an InSb infrared (IR) focal plane array camera operating at 60 Hz. The surface of the specimen was exposed to heat through a short pulse of light from a set of flash lamps. The IR camera was used to capture the temperature field of the specimen during and after the flash pulse for a predetermined period of time. SEM was

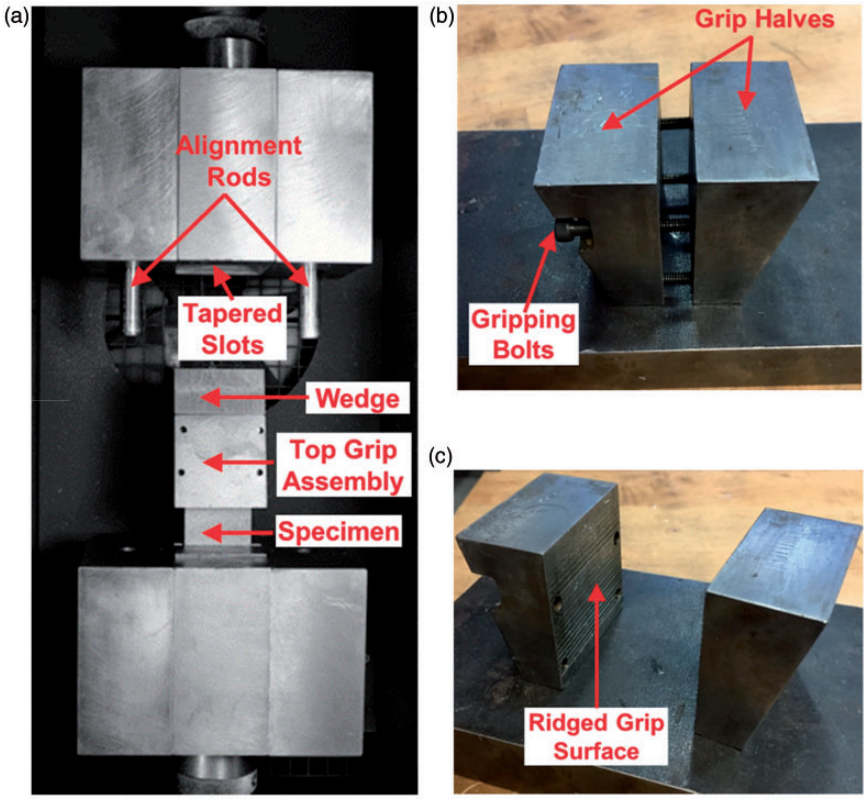

Figure 3. Modified ASTM D3410 compression fixture. (a) Installed fixture. (b) Threaded grip halves. (c) Separated grip halves.

performed in order to examine the modes of failure at different stress levels. The SEM used was a Hitachi S-4700 microscope and a low voltage was set (1–2 kV) to prevent damage on the surface of the specimen.

Experimental results

A minimum of five specimens were used for each type of test. The representative stress–strain plots for the axial and transverse tension specimens are presented in Figure 5. The axial tensile response is almost linear for all the specimens, but non-linear behavior was observed in the transverse direction. The braid angle and lack of tow continuity between the top and bottom grip surfaces in the transverse tension specimen are potential causes for the non-linear behavior as well as the lower elastic modulus and transverse strength. The edge effects located at the bias braid termination points in the transverse tension specimens cause premature damage such as subsurface axial tow splitting. For the transverse tensile response, the environmental conditions caused reductions in the proportional elastic limit (PEL) indicating macroscopic damage at lower strains. The average PEL strains for the room, hot, and hot/wet conditions are 0.95%, 0.81%, and 0.78%, respectively. A possible reason for the lower PEL strains and increased non-linearity in the

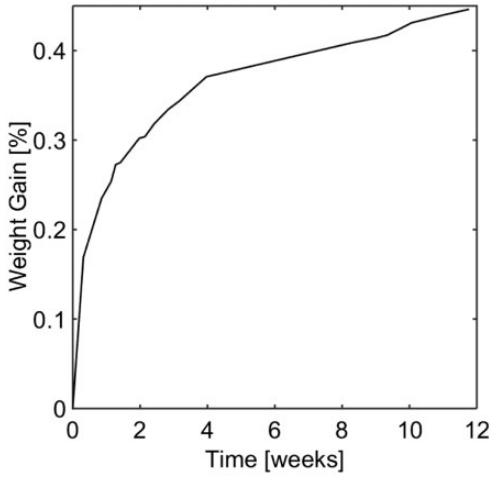

Figure 4. Average weight gain of the triaxial PMC due to moisture absorption.

transverse results is earlier axial tow splitting and this phenomenon is quantified later in this paper. The mean and standard deviation for the elastic and failure properties of the tensile tests are shown in Table 2. The mechanical properties for the room condition correlate well with properties and trends presented in previous studies.[11,18,32] Unlike the transverse tension direction,

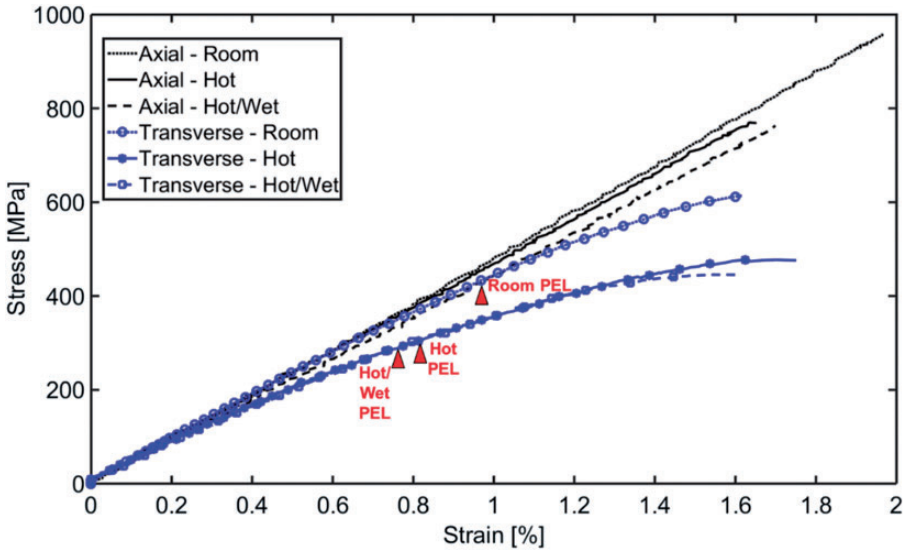

Figure 5. Representative stress-strain plots of tensile specimens (PEL points are indicated by red triangles and for references to color in this figure, the reader is referred to the web version of this article).

Table 2. Tension mechanical properties.

		Axial tension		Transverse tension	
Condition	Material parameter	Mean	Standard deviation	Mean	Standard deviation
Room condition	Failure stress (MPa)	936.33	43.83	609.83	10.67
	Failure strain (%)	2.00	0.05	1.69	0.20
	Modulus (GPa)	46.27	2.76	45.29	3.31
	Poisson's ratio	0.29	0.04	0.31	0.02
Hot	Failure stress (MPa)	755.70	57.82	464.97	17.71
	Failure strain (%)	1.65	0.09	1.75	0.13
	Modulus (GPa)	46.50	1.16	39.09	1.73
	Poisson's ratio	0.32	0.01	0.32	0.02
Hot/wet	Failure stress (MPa)	757.38	6.47	443.45	9.29
	Failure strain (%)	1.67	0.07	1.50	0.05
	Modulus (GPa)	45.13	1.01	40.53	1.45
	Poisson's ratio	0.32	0.02	0.34	0.03

the axial tensile results show that the environmental conditions affect the failure strength and Poisson's ratio with minimal effect on the elastic modulus. No significant difference was observed between the hot and hot/wet conditions.

Figure 6 (a) and (c) displays the major strain field of an axial and transverse tension specimen before failure, respectively, where the arrows indicate the major strain directions. The through-thickness and surface images presented in Figure 6 (b) and (d) show fiber breakage in axial tows for axial tension specimens and shear failure along the bias braid tows for transverse tensile specimens. The strain field on the axial specimens is non-uniform with local high-strain areas. The major strain directions show that the global strain was relatively parallel to the direction of loading, even in the local high-strain areas, and the edges of the axial specimens had almost no effect on the major strain directions. However, for transverse specimens, a distinct local strain pattern is evident along the edges of the specimen. The periodic strain pattern consists of a set of two high, closely spaced strain areas followed by a large semi-circular area of low strain. Other researchers have noted similar patterns using the out-of-plane

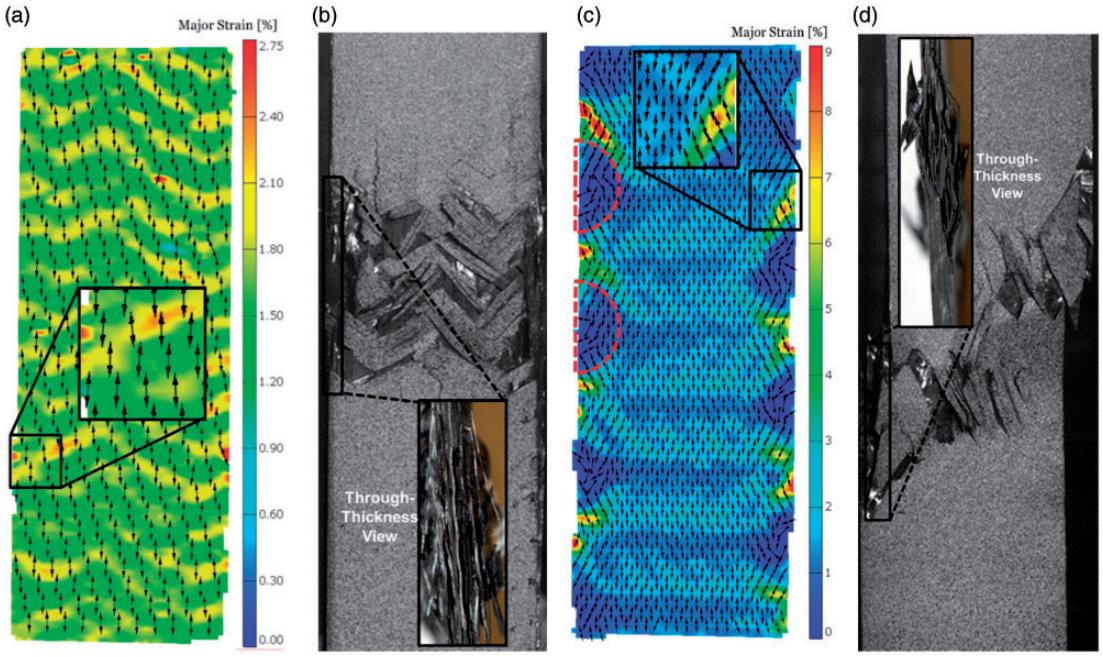

Figure 6. Images showing the major strain field just before failure, and the surface and through-thickness failure modes of a hot/wet conditioned axial tension specimen (a and b) and a hot conditioned transverse tension specimen (c and d) (For references to color in this figure, the reader is referred to the web version of this article).

deformation field[11,36] and the uniaxial strain field[11,18,32] for room condition. Zhang and Binienda[36] concluded that the pattern is caused by tension-torsion coupling due to the termination of bias braid tows at the edges of the specimen. Edge effects cause the strain to redirect around the semi-circular areas of low strain and this is shown by the major strain directions in the zoomed-in area of the transverse tensile strain field (Figure 6c). Although Figure 6 depicts the major strain contour of a hot conditioned transverse specimen, it is important to state that similar patterns are evident for each environmental condition. However, the strain level at the initial macroscopic damage as well as the intensity and size of the edge effects can differ between room and environmental conditions as discussed in the next section.

In order to quantify the effect of environmental conditions on the strain patterns and edge effects, a through-width strain distribution analysis was conducted. The major strain distribution was investigated at multiple cross sections by plotting the strain as a function of specimen width. The through-width strain data, for each environmental condition, was extracted at a stage that corresponded to the PEL strain to study macroscopic damage initiation. The through-width strain distribution at the PEL point is used to compare and investigate the possible causes of non-linearity at different environmental conditions in addition to the strain pattern and edge effects. The major strain results are presented as a function of width (Figure 7) for a hot conditioned, transverse tension specimen where the black curves represent the strain data extracted from sections of the strain field. The data were discretized with blue square points representing the major strain at the edges of the specimen where large strain gradients are prominent and red triangular points representing the strain at the center of the specimen where the values are approximately constant. The data provided from this analysis were used to compute α (indicating strain concentration) and β (indicating size of the edge effect) parameters which are defined by equations (1) and (2), respectively. It must be noted that the parameter β describes a ratio that directly represents the physical size of the edge effects, whereas the parameter α complements β by defining the intensity of the edge strain. Therefore, changes in the edge effects due to environmental conditions are best represented by the values of β

$$\alpha = \frac{\varepsilon_{edge}}{\varepsilon_{center}} \tag{1}$$

$$\beta = \frac{W_{edge}}{W_{center}} \tag{2}$$

In equations (1) and (2), ε_{edge} and ε_{center} represent the average values of major strain at the edge and the center of the specimen, respectively, and W_{edge} and W_{center} are the average calculated widths of the edge strain and center strain, respectively. The values for α and β for the axial and transverse tensile specimens are provided in Table 3. The α and β ratios show that the

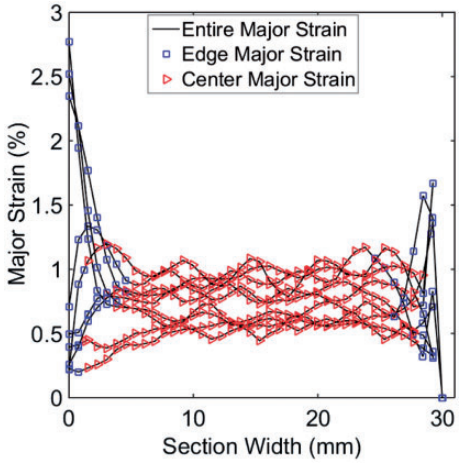

Figure 7. Through-width major strain distribution of a hot conditioned transverse tensile test (For references to color in this figure, the reader is referred to the web version of this article).

edge effects for the axial tension specimens are small and unaffected by the environmental conditions. On the contrary, the α and β values for the transverse tension direction demonstrate that the edge effects are critical and large for the environmental conditioned specimens. The possible causes for the larger size of edge effects in the transverse tensile specimens due to environmental conditions are increases in tow splitting damage.

The bowtie specimens were originally designed to mitigate the edge effects present in the transverse tension specimens.[33] The design of the notch for the bowtie specimen follows the angle of the braid to decrease the probability of a bias braid tow terminating at the edge. The major strain field in Figure 8 demonstrates that the edge effects along the specimen are minimal but concentrations still occur in the gage area near the notch tip due to the specimen geometry. The through-thickness and surface images illustrate failure associated with fiber breakage in the bias braid tows. The elastic and failure properties are presented in Table 4 and show that the bowtie moduli are larger than the axial and transverse moduli of the straight-sided specimens due to the complex tow architecture. In contrast to the transverse tension straight-sided specimen, bowtie specimens have tow continuity which allows the specimen to distribute the applied stress more effectively through the bias braid tows and provides larger strength values. The approximate schematic in Figure 9 illustrates the tow continuity, between grip surfaces, for the bowtie specimens as well as the bias braid termination that occurs in the transverse tensile straight-sided specimens. The architecture of the material is presented in Figure 10 and this cross section shows that the transverse direction contains more bias braid tows compared

Table 3. Tension strain distribution results.

Specimen type	Parameter	Room condition	Hot	Hot/wet
Axial tension	α	1.00	0.95	1.06
	β	0.05	0.07	0.09
Transverse tension	α	1.57	1.24	1.26
	β	0.17	0.28	0.77

to the number of axial tows in the axial direction. The tow continuity and larger number of bias tows produced the larger moduli measurements in the bowtie tests. The results obtained in this study and previous studies[32,33] show that another potential cause of the irregular moduli values is the multiaxial stress state at the notch tip of the specimen.

Representative axial and transverse compressive stress–strain plots of the triaxial braided composite are presented in Figure 11. Unlike the axial tensile response, the axial compression stress–strain response shows non-linear behavior. The major strain field and failure images presented in Figure 12 show that the non-linearity of the axial compression specimen was not caused by edge effects. The non-linearity of the axial compression specimens is attributed to the fiber microbuckling and shear failure modes which were not present in the axial tension specimens. The major strain contours show the existence of concentrations in the transverse compression specimen; although, these concentrations were not specifically located along the edge as in the transverse tension results. Furthermore, the through-width strain distribution results in Table 5 demonstrate that, similar to the axial tensile results, the size of the edge effects in the compression specimens is small with minimal changes due to the environmental conditions. The PEL strains for the axial and transverse compression response (Table 6) show that the environmental conditions cause damage at lower strains. The axial and transverse compressive strength, failure strain, modulus, and Poisson's ratio are summarized in Table 7. With the exception of the modulus, degradation of the mechanical properties was prevalent due to the environmental conditions.

The non-linear stress–strain plots for the shear specimens are shown in Figure 13 and the corresponding elastic and failure properties are given in Table 8. The presented shear properties for the room condition correlate well with the v-notched rail shear results obtained by Roberts et al.[11] The calculated PEL strains for the shear response were 1.18%, 0.87%, and 1.02% for the room, hot, and hot/wet conditions, respectively. The results show that the environmental conditions significantly affected the failure strength with only minor effects on the failure strain and shear modulus. Due to

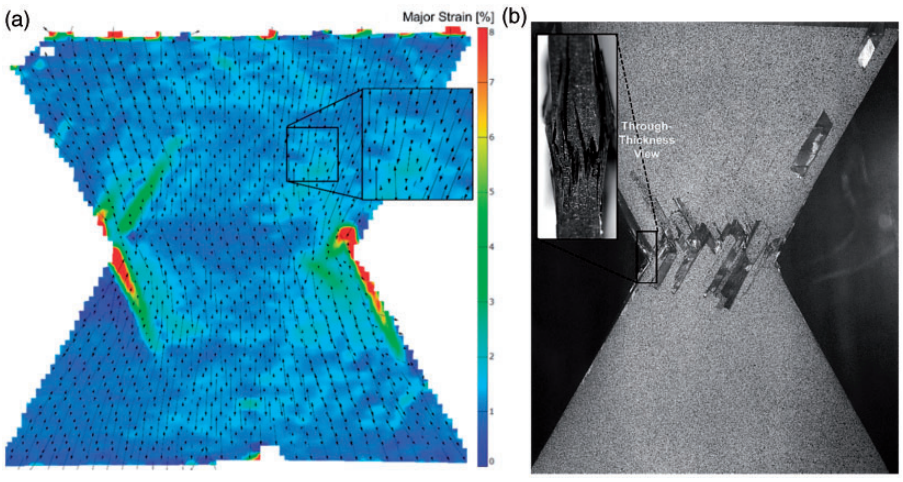

Figure 8. (a) The major strain field and directions and (b) the surface and through-thickness failure modes of a hot conditioned bowtie specimen (For interpretation of the color legend, the reader is referred to the web version of this article).

Table 4. Bowtie mechanical properties.

Condition	Material parameter	Mean	Standard deviation
Room condition	Failure stress (MPa)	803.17	64.06
	Modulus (GPa)	65.76	4.38
Hot	Failure stress (MPa)	771.97	75.59
	Modulus (GPa)	57.36	2.30
Hot/wet	Failure stress (MPa)	758.69	94.42
	Modulus (GPa)	55.84	2.16

the limited DIC viewing area of the shear specimen, the through-width strain distribution analysis was not performed for this response.

Failure analysis

Failure analysis was performed using a pulsed FT technique which uses two bulbs to apply heat to the surface of a specimen and an IR camera to capture temperatures contours of the specimen. In order to accurately perform the failure analysis, two unconditioned, untested specimens (defined as healthy specimens) were placed under the IR camera with the failed specimen to obtain reference data points. The EchoTherm software compiles images of the temperature contours of the specimens at specific time intervals during and after the flash from the bulbs. As shown in Figure 14(a), the temperature data can be computed from specific areas called cursors using the EchoTherm software and multiple cursors were used in random areas in the center of the specimen to average and extract data from the healthy and failed/damaged specimens. More detailed information regarding FT and the EchoTherm software can be found in

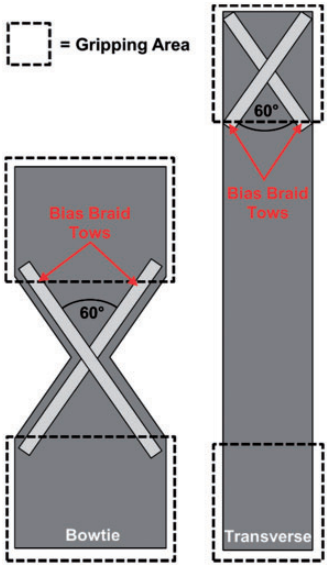

Figure 9. Bias braid tows in bowtie and transverse tension specimens.

the ASTM E2582 standard[37] and the EchoTherm manual.[38] Additionally, multiple pulsed flashes and data collection were conducted in order to get an appropriate number of data points for each damaged/failed specimen. For the failed specimens, cursor windows were placed over areas immediately adjacent to the failure region in order to determine the impact of loading on the overall structure of the specimen. The initial temperature value from each cursor window was subtracted from the subsequent values and logarithmic temperature-time plots were made to visualize the difference in thermography results between healthy and failed specimens (Figure 14b). Following the ASTM E2582 standard,[37] a line with a slope of –0.5 is overlaid

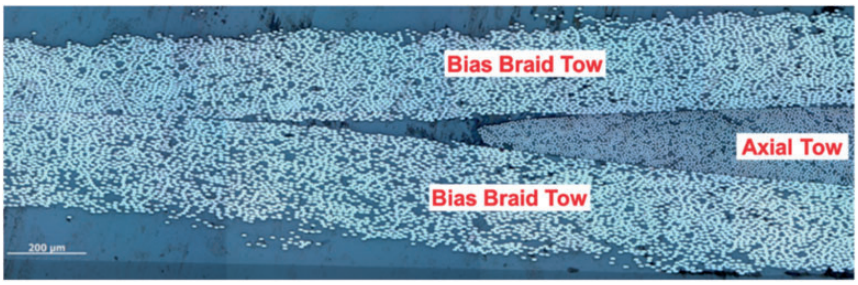

Figure 10. Optical micrograph of a transverse cross-section of the material (single lamina).

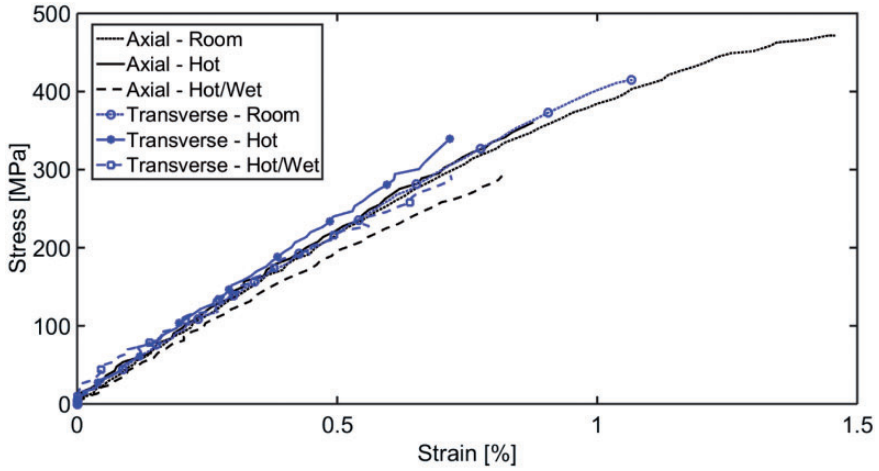

Figure 11. Representative stress–strain plots of axial and transverse compression specimens.

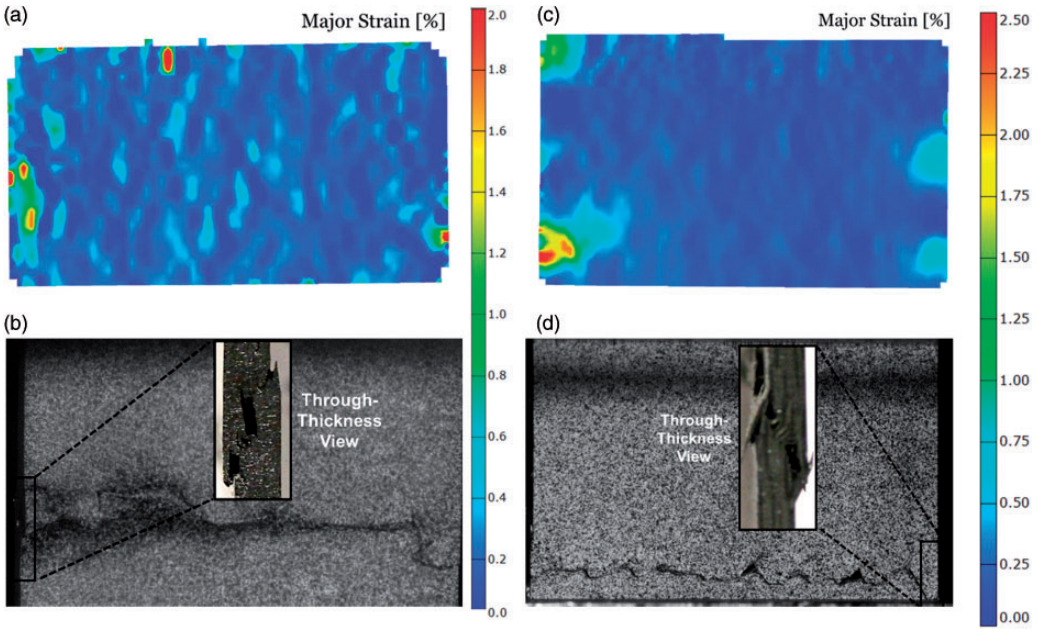

Figure 12. Major strain contours and failure images of hot/wet conditioned axial and transverse compression tests (For interpretation of the color legends, the reader is referred to the web version of this article). (a) Axial compression contour. (b) Axial compression failure. (c) Transverse compression contour. (d) Transverse compression failure.

starting at the descent of these curves and any deviations from this slope represent defects/damages within the material. For the analysis in this study, the area under the temperature-time curves was used and the ratio of healthy area to damaged area at the center of each specimen is defined as the damage metric (referred to as central damage). The center area of the specimen was used to reduce the effect of edges. The damage metric was also applied to determine the effects that environmental conditioning and loading have at the edges of the specimen (referred to as edge/center damage). This edge/center damage value is the ratio of the edge area to the central area of the temperature-time plot; where the edge area was extracted using cursor windows placed near the edge of the specimens.

Several specimens were loaded to lower stress levels to induce damage without failure. These results were used to better quantify damage progression as presented in Figure 15 and Figure 16. The edge/damage ratio for the healthy state was approximately 1.24 and this initial concentration was caused by damage induced during fabrication of the specimens and also due to the boundary effects during the FT procedure. The healthy state of a specimen has a value of 100% and any deviations from this value

Table 5. Compression strain distribution results.

Specimen type	Parameter	Room condition	Hot	Hot/wet
Axial compression	α	1.4	1.3	1.85
	β	0.11	0.15	0.11
Transverse compression	α	2.8	2.4	2.7
	β	0.10	0.14	0.16

Table 6. Compression PEL strains.

	Room	Hot	Hot/wet
Axial compression	0.98%	0.62%	0.65%
Transverse compression	0.87%	0.62%	0.60%

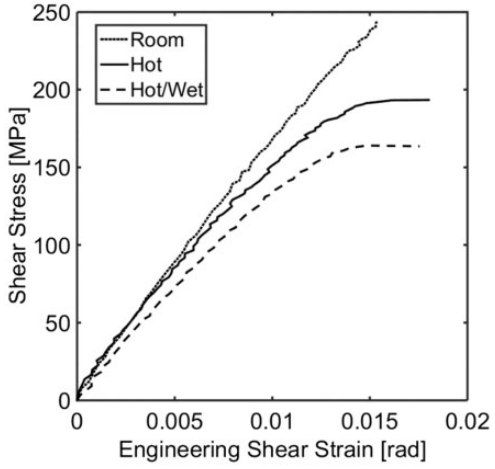

Figure 13. Representative shear stress–strain response.

Table 7. Compression mechanical properties.

		Axial compression		Transverse compression	
Condition	Material parameter	Mean	Standard deviation	Mean	Standard deviation
Room condition	Failure stress (MPa)	456.04	37.11	393.08	21.87
	Failure strain (%)	1.39	0.10	1.02	0.10
	Modulus (GPa)	43.98	1.35	45.12	0.77
	Poisson's ratio	0.31	0.01	0.31	0.01
Hot	Failure stress (MPa)	317.85	30.63	311.67	20.81
	Failure strain (%)	0.80	0.04	0.81	0.09
	Modulus (GPa)	44.41	2.50	45.36	3.04
	Poisson's ratio	0.30	0.04	0.32	0.02
Hot/wet	Failure stress (MPa)	279.22	14.63	274.18	26.19
	Failure strain (%)	0.75	0.11	0.66	0.07
	Modulus (GPa)	43.35	1.76	46.56	1.54
	Poisson's ratio	0.35	0.03	0.31	0.06

Table 8. In-plane shear mechanical properties.

Condition	Material parameter	Mean	Standard deviation
Room condition	Failure stress (MPa)	250.51	7.87
	Failure strain (%)	1.87	0.16
	Modulus (GPa)	17.14	0.94
Hot	Failure stress (MPa)	186.83	14.17
	Failure strain (%)	1.67	0.20
	Modulus (GPa)	15.85	1.17
Hot/wet	Failure stress (MPa)	177.04	13.29
	Failure strain (%)	1.50	0.12
	Modulus (GPa)	14.45	0.80

represent center damage in the specimen. The deviations in the edge/center ratios (shown in Figure 15) for the damaged axial tension specimens demonstrate negligible effects due to the edges. These edge/center ratios verify the through-width strain distribution results in Table 3 and indicate that premature damage due to tow splitting was not apparent. For the failed specimens at room and environmental conditions, the edge/center ratios increased above 1.4 likely due to stress waves caused by the sudden failure of the specimen.

The FT analysis for the transverse tensile specimens shows markedly different trends than that of the axial tension. The transverse tensile results in Figure 16 show

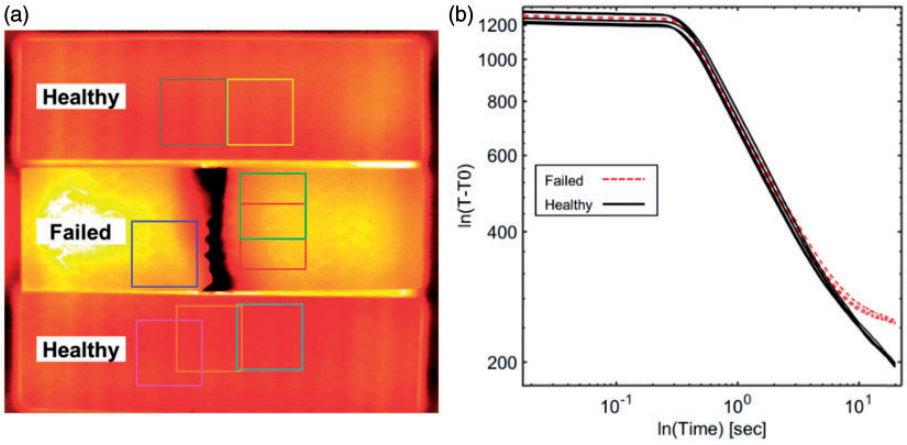

Figure 14. (a) Multiple cursor windows overlaid on an FT contour and (b) a logarithmic plot of temperature-time data for healthy and failed axial compression specimens (For references to color in this figure, the reader is referred to the web version of this article).

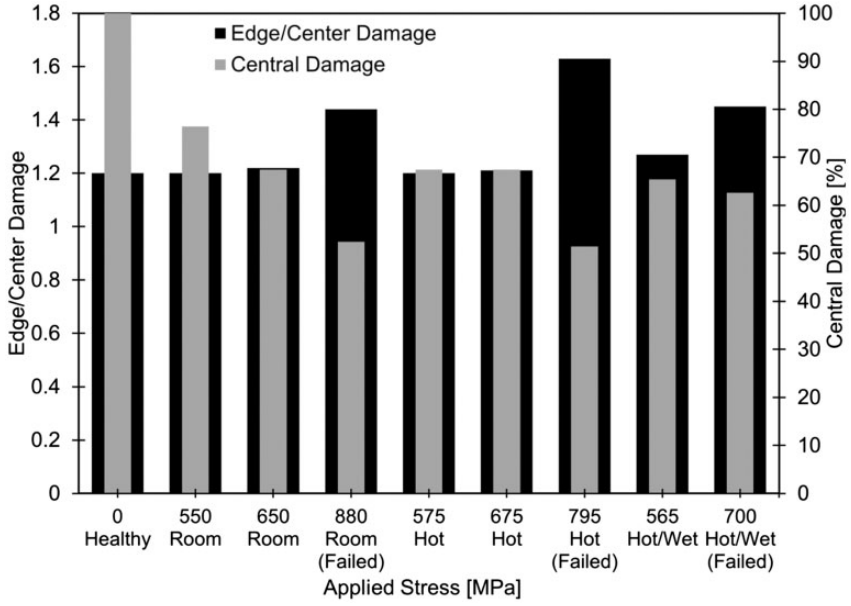

Figure 15. Thermography analysis of the axial tensile specimens.

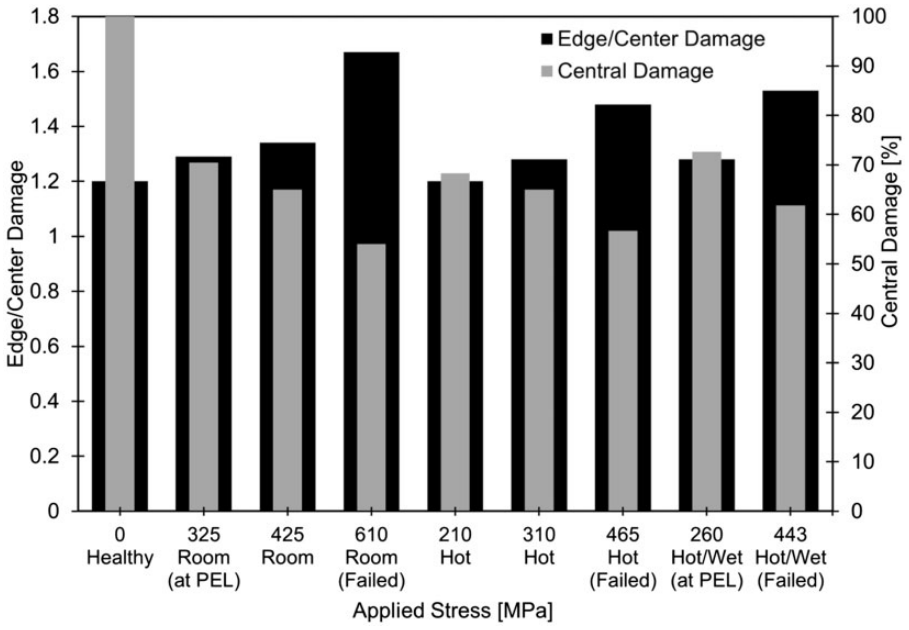

Figure 16. Thermography analysis of the transverse tensile specimens.

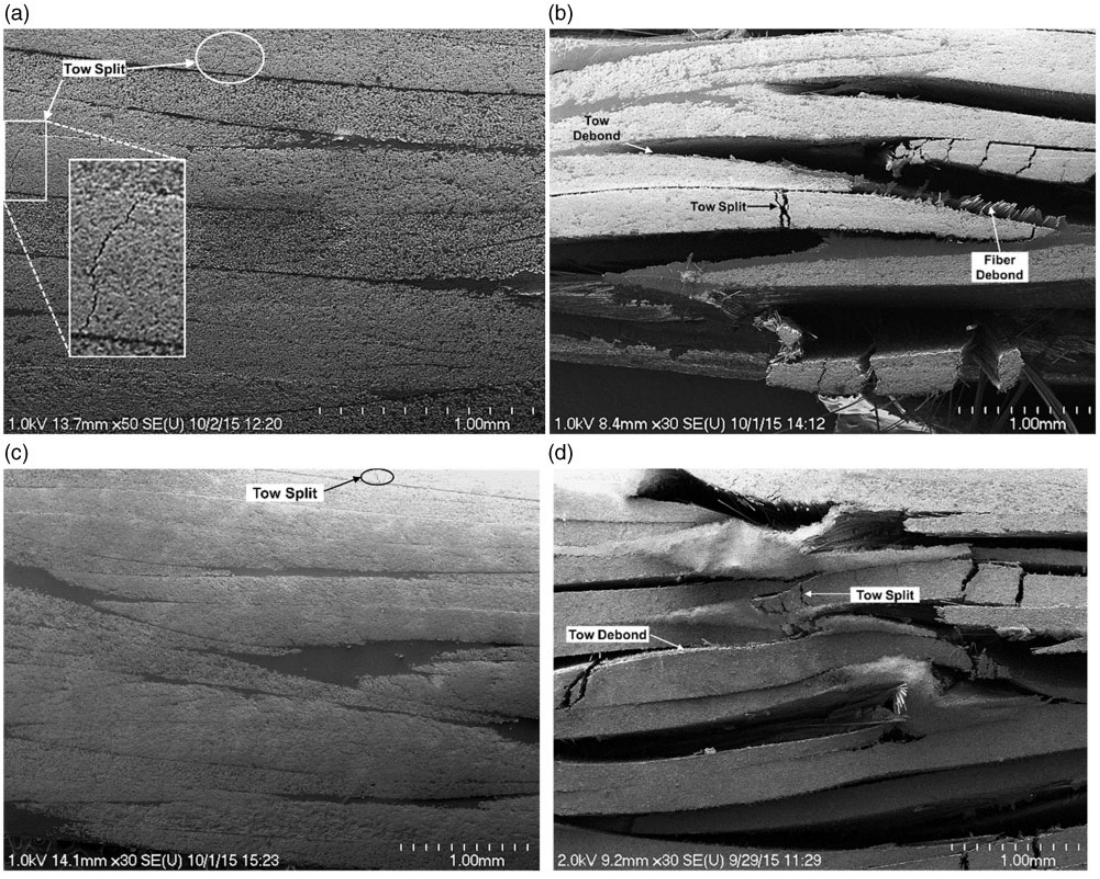

Figure 17. SEM images of transverse tensile specimens under environmental conditions. (a) Hot condition (310 MPa). (b) Hot condition (failed). (c) Hot/wet condition (260 MPa). (d) Hot/wet condition (failed).

larger edge/center ratios between the damage and healthy states. Specifically, the results show larger edge/center ratios for specimens loaded to PEL and after PEL which indicate the occurrence of progressive damage at the edge of the specimen potentially due to increased splitting of the subsurface axial tows. The increased edge/center ratios correlate with the through-width strain distribution results in Table 3 which showed that strain concentrations occurred at the edges for specimens loaded to the PEL point. A comparison of the environmental conditions with the room condition demonstrates that, for similar stress levels, the environmental conditions had larger edge/center ratios. The central damage percentages show that the environmentally conditioned specimens were more susceptible to damage. SEM was performed on damaged and failed transverse tensile specimens to study damage initiation and propagation in the material. Micrographs of hot and hot/wet conditioned specimens, loaded to PEL, (Figure 17) show that tow splitting is the initial failure mechanism. For failed specimens, failure modes such as tow and fiber debonding are present in addition to tow splitting. The tow splitting in the bottom-right of Figure 17(b) demonstrates that the split initiates at the edge and increases at the edge as well as grows through the width of the specimen.

Concluding remarks

The current study examined the effects of hot (100°C) and hot/wet conditions (60°C/90% RH) on the mechanical properties and failure of triaxial braided composites under tension, compression, and shear loads. A decrease in failure stress by approximately 19% was observed for tension, compression, and shear when comparing the environmental conditions with room condition as the reference. Results show that an increase in temperature is a driving factor for the degradation of the material parameters. The through-width strain distribution results demonstrated that strain concentrations exist on the edges and the size of these edge effects increases with environmental conditions. This conclusion was verified with the FT analysis which inspected the damage in the center and at the edges of each specimen. The SEM showed similar damage propagation mechanisms for both hot and hot/wet conditions where damage initiated in the form of tow splitting and total failure was a combination of failure modes including tow splitting, tow debonding, and fiber debonding.

Declaration of Conflicting Interests

The author(s) declared no potential conflicts of interest with respect to the research, authorship, and/or publication of this article.

Funding

The author(s) disclosed receipt of the following financial support for the research, authorship, and/or publication of this article: This project was supported by the Governor's Office of Economic Recovery and Science Foundation Arizona, Vice President for Research: Dr. Gary Greenburg, Agreement Number: SRG 0443-10. The authors would also like to acknowledge Honeywell Aerospace for providing all the specimens and for equal cost share for this research.

References

1. Patel SR and Case SW. Durability of hygrothermally aged graphite/epoxy woven composite under combined hygrothermal conditions. *Int J Fatigue* 2002; 24: 1295–1301.
2. Adams RD and Singh MM. The dynamic properties of fibre-reinforced polymers exposed to hot, wet conditions. *Compos Sci Technol* 1996; 56: 977–997.
3. Bishop SM. The mechanical performance and impact behaviour of carbon-fibre reinforced PEEK. *Compos Struct* 1985; 3: 295–318.
4. Choi HS, Ahn KJ, Nam J-D, et al. Hygroscopic aspects of epoxy/carbon fiber composite laminates in aircraft environments. *Compos A Appl Sci Manufact* 2001; 32: 709–720.
5. Collings TA, Harvey RJ and Dalziel AW. The use of elevated temperature in the structural testing of FRP components for simulating the effects of hot and wet environmental exposure. *Composites* 1993; 24: 625–634.
6. Suh D-W, Ku M-K, Nam J-D, et al. Equilibrium water uptake of epoxy/carbon fiber composites in hygrothermal environmental conditions. *J Compos Mater* 2001; 35: 264–278.
7. Joshi OK. The effect of moisture on the shear properties of carbon fibre composites. *Composites* 1983; 14: 196–200.
8. Zhang C, Binienda WK, Morscher GN, et al. Experimental and FEM study of thermal cycling induced microcracking in carbon/epoxy triaxial braided composites. *Compos A Appl Sci Manufact* 2013; 46: 34–44.
9. Schambron T, Lowe A and McGregor HV. Effects of environmental ageing on the static and cyclic bending properties of braided carbon fibre/PEEK bone plates. *Compos B Eng* 2008; 39: 1216–1220.
10. Kohlman LW, Roberts GD, Miller SG, et al. Investigation of hygro-thermal aging on carbon/epoxy materials for jet engine fan sections, http://ntrs.nasa.gov/archive/nasa/casi.ntrs.nasa.gov/20110014484.pdf (accessed 14 June 2015).
11. Roberts GD, Goldberg RK, Binienda WK, et al. Characterization of triaxial braided composite material properties for impact simulation. *NASA TM* 2009; 215660: 2009.
12. Masters JE and Ifju PG. A phenomenological study of triaxially braided textile composites loaded in tension. *Compos Sci Technol* 1996; 56: 347–358.
13. Portanova MA. *Standard methods for unnotched tension testing of textile composites*. National Aeronautics

and Space Administration, Langley Research Center, 1995.
14. Masters JE, Foye RL, Pastore CM, et al. Mechanical properties of triaxially braided composites: experimental and analytical results. *J Compos Technol Res* 1993; 15: 112–122.
15. Potluri P, Manan A, Francke M, et al. Flexural and torsional behaviour of biaxial and triaxial braided composite structures. *Compos Struct* 2006; 75: 377–386.
16. Naik RA, Ifju PG and Masters JE. Effect of fiber architecture parameters on deformation fields and elastic moduli of 2-D braided composites. *J Compos Mater* 1994; 28: 656–681.
17. Yekani Fard M, Liu Y and Chattopadhyay A. Characterization of epoxy resin including strain rate effects using digital image correlation system. *J Aerospace Eng* 2011; 25: 308–319.
18. Littell J, Roberts GD and Goldberg RK. Characterization of damage in triaxial braided composites under tensile loading. *J Aerospace Eng* 2009; 22: 270–279.
19. Rao YJ, Yuan SF, Zeng XK, et al. Simultaneous strain and temperature measurement of advanced 3-D braided composite materials using an improved EFPI/FBG system. *Optic Laser Eng* 2002; 38: 557–566.
20. Ching Quek S, Waas AM, Shahwan KW, et al. Compressive response and failure of braided textile composites: Part 1—experiments. *Int J Non-Linear Mech* 2004; 39: 635–648.
21. Smith LV and Swanson SR. Failure of braided carbon/epoxy composites under biaxial compression. *J Compos Mater* 1994; 28: 1158–1178.
22. Ivanov DS, Baudry F, Van Den Broucke B, et al. Failure analysis of triaxial braided composite. *Compos Sci Technol* 2009; 69: 1372–1380.
23. Lomov SV, Ivanov DS, Truong TC, et al. Experimental methodology of study of damage initiation and development in textile composites in uniaxial tensile test. *Compos Sci Technol* 2008; 68: 2340–2349.
24. Sun JG, Deemer C, Ellingson WA, et al. *Thermal imaging measurement and correlation of thermal diffusivity in continuous fiber ceramic composites*. Argonne National Lab., IL (United States), 1997.
25. Maldague XP. Introduction to NDT by active infrared thermography. *Mater Eval* 2002; 60: 1060–1073.
26. Shepard SM, Hou Y, Ahmed T, et al. Reference-free interpretation of flash thermography data. *Insight-Non-Destruct Test Cond Monitor* 2006; 48: 298–301.
27. Yekani Fard M, Sadat SM, Raji BB, et al. Damage characterization of surface and sub-surface defects in stitch-bonded biaxial carbon/epoxy composites. *Compos B Eng* 2014; 56: 821–829.
28. ASTM D3171. *Standard test methods for constituent content of composite materials*. American Society for Testing and Materials: West Conshohocken, PA, 2006.
29. ASTM D3410/D3410M 2003 (2008). *Standard test method for compressive properties of polymer matrix composite materials with unsupported gage section by shear loading*. American Society for Testing and Materials: West Conshohocken, PA, 2003.
30. ASTM D3039. *Standard test method for tensile properties of polymer matrix composite materials*. American Society for Testing and Materials: West Conshohocken, PA, 2003.
31. ASTM D7078. *Standard test method for shear properties of composite materials by v-notched rail shear method*. American Society for Testing and Materials: West Conshohocken, PA, 2004.
32. Kohlman LW, Bail JL, Roberts GD, et al. A notched coupon approach for tensile testing of braided composites. *Compos A Appl Sci Manufact* 2012; 43: 1680–1688.
33. Bowman CL, Roberts GD, Braley MS, et al. Mechanical properties of triaxial braided carbon/epoxy composites. *NASA TM 2003*; 0113144: 2003.
34. Aramis GOM. *Theory and user manual*; *2006*.
35. ASTM D5229. *Standard test method for moisture absorption properties and equilibrium condition of polymer matrix composite materials*. American Society for Testing and Materials: West Conshohocken, PA, 2004.
36. Zhang C and Binienda WK. Numerical analysis of free-edge effect on size-influenced mechanical properties of single-layer triaxially braided composites. *Appl Compos Mater* 2014; 21: 841–859.
37. ASTM E2582-07,2007. *Standard practice for infrared flash thermography of composite panels and repair patches used in aerospace applications*. American Society for Testing and Materials: West Conshohocken, PA, 2007.
38. Thermal Wave Imaging. *EchoTherm User Manual*; 2004.